JGR Space Physics

RESEARCH ARTICLE
10.1029/2023JA032101

The Influence of Rotational Discontinuities on the Formation of Reconnected Structures at Collisionless Shocks—Hybrid Simulations

K. Steinvall[1] **and I. Gingell**[1]

[1]School of Physics and Astronomy, University of Southampton, Southampton, UK

Key Points:

- Bursts of magnetic reconnection can occur when upstream rotational discontinuities interact with collisionless shocks
- The occurrence of reconnection favors quasi-parallel shocks and rotational discontinuities with large magnetic shear
- The increased reconnection is associated with foreshock bubbles and reconnection of the rotational discontinuity itself

Correspondence to:
K. Steinvall,
L.K.G.Steinvall@soton.ac.uk

Citation:
Steinvall, K., & Gingell, I. (2024). The influence of rotational discontinuities on the formation of reconnected structures at collisionless shocks—Hybrid simulations. *Journal of Geophysical Research: Space Physics*, *129*, e2023JA032101. https://doi.org/10.1029/2023JA032101

Received 19 SEP 2023
Accepted 4 JAN 2024

Abstract Recent simulations and in-situ observations have shown that magnetic reconnection is an active dissipation mechanism in the transition region of collisionless shocks. The generation mechanisms and upstream conditions enabling reconnection have been studied numerically. However, these numerical studies have been limited to the case of a steady, uniform upstream. The effect upstream discontinuities have on shock reconnection remains poorly understood. Here, we use local hybrid (fluid electron, particle ion) simulations with time-varying upstream conditions to study the influence upstream rotational discontinuities (RDs) have on the formation of reconnected magnetic structures in the shock transition region. Our results show that bursts of reconnection can occur when RDs interact with the shock. This effect is much more significant at initially quasi-parallel shocks than quasi-perpendicular shocks, as the interaction between the RDs and the foreshock (only present in the quasi-parallel case) can lead to the generation of foreshock bubbles, in which we observe an enhanced reconnection occurrence. The enhanced fluxes of accelerated ions within the foreshock bubble are likely a contributing factor to the increased reconnection occurrence. In addition, we find that the RDs with large magnetic shear are prone to reconnect upon reaching the shock, resulting in the generation of large magnetic islands. Our findings illustrate that upstream discontinuities can significantly increase the amount of reconnected magnetic structures at the bow shock, suggesting that reconnection might be a particularly important dissipation mechanism during periods of dynamic upstream conditions.

1. Introduction

Collisionless shock waves are common throughout the universe in different astrophysical and space plasma contexts where fast (super-Alfvénic) flows are present. They are found at supernova remnants, coronal mass ejections, and planets (Burgess & Scholer, 2015). The collisional mean free path of particles in such plasmas tends to be much larger than the plasma scales, and Coulomb collisions do not contribute significantly to the bulk deceleration and heating of the supersonic plasma across the shock. Instead, energy is dissipated via kinetic processes (e.g., Burgess & Scholer, 2015; Kennel et al., 1985).

Recent spacecraft observations have revealed that magnetic reconnection (e.g., Birn & Priest, 2007; Hesse & Cassak, 2020) frequently occurs inside thin current sheets at the Earth's bow shock, potentially contributing significantly to energy dissipation and particle acceleration (Gingell et al., 2019, 2020; Wang et al., 2019). In-situ measurements have estimated that thin current sheets, not distinguishing between reconnecting and non-reconnecting, may be responsible for processing up to 11% of the solar wind ram energy in the Earth's magnetosheath (Schwartz et al., 2021). The mechanism generating these current sheets is different depending on plasma and shock parameters such as the plasma β, the Alfvénic Mach number M_A, and the angle θ_{Bn} between the shock normal vector and the upstream magnetic field (Bessho et al., 2020; Gingell et al., 2017; Matsumoto et al., 2015).

Using 2D particle-in-cell (PIC) simulations of quasi-parallel ($Q_{\parallel}$; $\theta_{Bn} < 45°$) shocks with parameters representative of the Earth's bow shock ($\beta = 1, M_A \in \{6, 11\}$), Bessho et al. (2020) showed that the presence of reconnecting current sheets is intimately connected to kinetic instabilities driving electromagnetic waves in the ion foreshock and shock foot. The reservoir of free energy provided by the solar-wind-shock system enables the waves to grow to large enough amplitudes that the magnetic field becomes highly distorted, forming thin current sheets which can undergo magnetic reconnection (see Figure 8 in Bessho et al., 2020). In a recent follow-up study, Bessho et al. (2023) showed that the resulting ion-scale magnetic islands are able to accelerate trapped electrons to high energies.

A necessary ingredient for the growth of these instabilities is a counter streaming beam formed by shock-reflected ions at $Q_{\parallel}$ shocks (Bessho et al., 2020; Gingell et al., 2017). Such beams are not present at quasi-perpendicular ($Q_{\perp}$; $\theta_{Bn} > 45°$) shocks, and fewer reconnecting current sheets are thus expected in that case. Indeed, a recent study by Gingell et al. (2023) found that this is the case in hybrid simulations. Their results showed that the occurrence of reconnection in the region upstream of the shock increases for decreasing θ_{Bn} and increasing M_A. Moreover, they found that reconnection stops almost entirely for $\theta_{Bn} > 50°$. In contrast to the hybrid simulations, reconnecting thin current sheets are universally observed by spacecraft in the shock transition region (Gingell et al., 2020), although primarily in the so called electron-only mode (e.g., Califano et al., 2020; Phan et al., 2018), which does not exist in hybrid models. Such electron-scale reconnection has been observed in 2D full PIC simulations of $Q_{\perp}$ shocks (A. Guo et al., 2023; Lu et al., 2021). These contrasting results emphasize the importance of studying the physics of both small and large scales to get a complete understanding of shock physics. In the present paper, we focus on the ion-physics of the ion-scales.

One important limitation of the aforementioned numerical models is that they enforced steady and uniform upstream conditions. In contrast, the solar wind is highly dynamic in nature and generally contains large current sheets corresponding to magnetic field discontinuities (e.g., Burlaga et al., 1977; Knetter et al., 2004; Vasko et al., 2022). The arrival of solar wind discontinuities to the bow shock can lead to the formation of foreshock transients such as hot flow anomalies (HFAs) and foreshock bubbles (FBs) (see the review by Zhang et al., 2022, and references therein). The dynamics produced inside such transients have been found to trigger local magnetic reconnection on the scale of around 1 ion inertial length, d_i (Liu et al., 2020), suggesting a potential ion response. In addition, hybrid simulations and in-situ observations have shown that the compression of current sheets upon impact with the bow shock can cause them to reconnect on large scales (Hamrin et al., 2019; Lin, 1997). Observations of ion-scale flux ropes inside foreshock transients have provided further evidence that magnetic reconnection can be triggered by the interaction between upstream discontinuities and shocks (Bai et al., 2020). What these studies show is that we need to consider the effects of upstream discontinuities in order to get a complete picture of the role magnetic reconnection plays at collisionless shocks.

While there are plenty of published studies that have used hybrid simulations to investigate the interaction between solar wind discontinuities and the Earth's magnetosphere/bow shock (e.g., Z. Guo et al., 2021; Lin, 1997; Omidi & Sibeck, 2007; Omidi et al., 2010, 2020), they have mainly relied on global models. The large scope of such models makes them computationally expensive, and exploring the massive parameter space associated with discontinuity-shock-interactions using global models is impractical. In addition, the focus of the previous studies has, with a few exceptions (e.g., Karimabadi et al., 2014), primarily been on either the formation of foreshock transients, or on the magnetospheric response to upstream discontinuities, leaving the topic of magnetic reconnection at the shock largely unexplored.

In the present paper, we use a local hybrid model to study the occurrence of ion-scale reconnection due to the interaction between upstream rotational discontinuities (RDs) and collisionless shocks. In particular, we aim to answer the question: is the formation of reconnected structures enhanced during shock restructuring due to upstream RDs? We find that the response depends strongly on the initial shock and RD properties. The most significant response is observed when an RD with large magnetic shear interacts with a $Q_{\parallel}$ shock. In this case, the formation of a foreshock bubble and internal reconnection of the RD results in a dramatic increase of reconnected magnetic field. In contrast, we find that the shock-RD interaction only marginally modulates the occurrence of reconnected structures in the case of an initially $Q_{\perp}$ shock.

2. Methods

2.1. Numerical Model

The model we use in this study is a modified version of the 2.5D hybrid-PIC model used by Gingell et al. (2023), which, in turn, is based on the fully kinetic PIC code EPOCH (Arber et al., 2015). In the hybrid model (Matthews, 1994), ions are treated as macro-particles and electrons as a massless, charge-neutralizing fluid. We are thus able to explore the kinetic ion physics we are interested in, while minimizing the computational cost. By not having to resolve the electron scales, we are also able to use a much larger simulation domain compared to a full PIC simulation using the same computational resources. Using the hybrid approach, we are therefore able to get a better picture of the evolution of the system, especially deeper into the magnetosheath and further out into the foreshock.

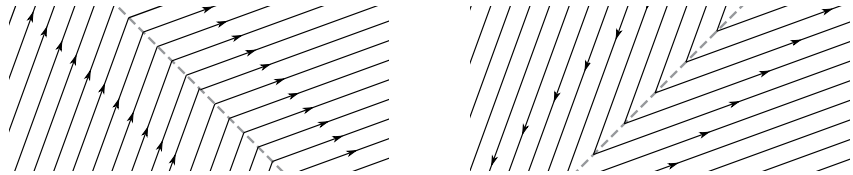

Figure 1. Schematic showing magnetic field lines of two RDs with different magnetic shear (left: $\Delta\varphi_B = 50°$, right: $\Delta\varphi_B = 130°$), resulting in the same θ_{Bn} transition from 20° to 70° for a vertical shock surface located to the right of the RDs.

Space is resolved in two dimensions (x, y) while the electromagnetic fields and currents are three dimensional. Our code allows for time varying inflow conditions, which enables us to introduce upstream discontinuities once the shock is well developed. The simulation grid is defined by (N_x, N_y) = (800, 800) square cells of side length $\Delta x = \Delta y = 0.15 d_i$ (using the upstream d_i), such that the simulation domain has lengths (L_x, L_y) = (120, 120)d_i. We are thus focusing on a limited part of the shock, neglecting the global scales. Each cell is initialized with 100 macro-particles. The simulation boundaries are defined as follows. At $x = 0$, plasma flows into the simulation domain with a time-dependent magnetic field, enabling us to introduce discontinuities. At $x = L_x$, particles are reflected to initialize the shock. In contrast to Gingell et al. (2023), who used periodic boundaries at $y = 0$ and $y = L_y$, we use boundaries that are open for electromagnetic fields ($\partial/\partial y = 0$), and act as a thermal reservoir for particles. Each particle that leaves the domain through these boundaries is replaced by a particle randomly drawn from a Maxwellian distribution function with equal temperature (T) and flow velocity v_x to the bordering cell. This change is necessary for the model to treat discontinuities with arbitrary normal vectors, as such discontinuities are incompatible with periodic boundary conditions. To limit the influence of edge effects, we perform our analysis in a smaller box in the center of the domain, $30 \leq y/d_i \leq 90$. In addition, we inject the RDs at times such that the shock-RD interaction takes place after the shock is first well developed. We judge the shock to be well developed once the $x = L_x$ boundary is no longer influencing the dynamics at the shock, and, for the $Q_\parallel$ shocks, when they have undergone shock reformation. Typically we find that the shock is well developed after $t \approx 20\omega_{ci}^{-1}$, where ω_{ci} is the angular ion cyclotron frequency. We stop the simulations before edge effects start influencing the physics within the smaller box.

2.2. Run Descriptions

The main aim of this study is to gain insight into how upstream magnetic field rotations associated with RDs affect the occurrence of magnetic reconnection and thus formation of magnetic islands in the shock transition region. We choose to focus on RDs which change the shock geometry significantly, $Q_\parallel \leftrightarrow Q_\perp$, as this leads to the most dramatic restructuring of the shock. To this end, we perform a series of simulations with upstream RDs which change the shock geometry from $Q_\parallel$ with $\theta_{Bn} = 20°$, to $Q_\perp$ with $\theta_{Bn} = 70°$ or vice versa. Depending on the RD properties, there are different ways of achieving these changes in θ_{Bn}. For simplicity, we will only consider RDs across which the tangential magnetic field with respect to the RD rotates by 180°. We use the following functional form in the RD's local coordinate system (x', y', z'): $B_{x'} = B_n$, $B_{y'} = B_t \cos(\theta(x'))$, $B_{z'} = B_t \sin(\theta(x'))$, where B_n and B_t are the magnetic field components normal and tangential to the RD respectively, and $\theta(x') = \left[1 + \tanh\left(\frac{x'-x'_0}{L_{RD}}\right)\right]\pi/2$, with x'_0 being the position of the RD and L_{RD} the half-width (e.g., Richter & Scholer, 1989). For such RDs, there are different orientations which give the desired θ_{B_n} changes. Here, we will only analyze the minimum and maximum magnetic shear ($\Delta\varphi_B$) configurations, corresponding to $\Delta\varphi_B = 50°$ and $\Delta\varphi_B = 130°$, respectively, which are illustrated in Figure 1. All RDs used in this study have $L_{\mathrm{RD}} = 3d_i$, a value common for current sheets at 1 AU (Vasko et al., 2022). We summarize our simulation runs in Table 1. In all cases, we use an upstream plasma beta $\beta_0 = 1$, and the initial magnetic field lies in the xy-plane. We include two runs (Run 6 and 7) without RDs to provide reference points for the $Q_\parallel$ shock geometry. Run 7 uses periodic y-boundaries so that we can ensure that our choice of boundary conditions do not affect the results significantly. We do not include any $Q_\perp$ reference runs since, as we will later see, reconnection is practically non-existent in those runs.

Table 1
Shock and RD Parameters for the Simulations Included in This Study

Run ID	$\theta_{Bn,0}$ [°]	$\theta_{Bn,1}$ [°]	$\Delta\varphi_B$ [°]	U_{in}/v_A	M_A
Run 1	70	20	50	6	8.4
Run 2	70	20	130	6	8.4
Run 3	20	70	50	6	7.8
Run 4	20	70	130	6	7.8
Run 5	20	70	130	9	12.3
Run 6[a]	20	20	–	6	7.8
Run 7[a,b]	20	20	–	6	7.8

Note. The $\theta_{Bn,0}$ and $\theta_{Bn,1}$ values are evaluated downstream and upstream of the RDs, respectively. The inflow velocity U_{in} is normalized to the upstream Alfvén velocity v_A, and the Alfvén Mach number M_A value is evaluated prior to the shock-RD interaction.

[a]Reference runs without RDs. [b]Periodic y-boundaries.

2.3. Quantifying Magnetic Reconnection

To quantify the occurrence of magnetic reconnection, we use the method of Gingell et al. (2023). In short, the method is based on the fact that magnetic reconnection in 2D necessarily creates closed field structures, that is, magnetic islands. By counting the number of closed field structures or the area occupied by them, we gain insight into how much reconnection has occurred. In order to determine whether or not a grid cell in the simulation contains closed flux at a given time t, we use the magnetic field lines starting at the simulation boundaries as probes. From these boundaries, we integrate 100 uniformly spaced lines per cell. If no closed flux is present in the entire simulation domain, the probing field lines will pass through every single grid cell. If, conversely, there exists one or more magnetic island in the domain, then the grid cells these islands occupy are inaccessible to the probing field lines. Thus, by keeping track of the cells crossed by the probing lines we can construct a binary map $M(x, y, t)$ which flags whether a given grid cell (x_i, y_j) contains closed flux, $M(x_i, y_j, t) = 1$, or open flux, $M(x_i, y_j, t) = 0$ at a given time. By stepping through the grid, we compute the total area occupied by closed magnetic flux as $A_{\text{closed}}(t) = \sum_{ij} M(x_i, y_j, t)\Delta x \Delta y$.

Due to the grid discretization, there is a tendency for the probing lines (which are obtained by integrating the magnetic field **B**) to occasionally bunch up. The gap between such bunches form thin streaks which are misidentified as containing closed flux. Unlike the magnetic islands produced by reconnection which are somewhat circular, these streaks appear as approximately 1D lines and are thus easily identified and removed from the analysis. Another issue occurs when closed flux is present at the simulation boundary. Some probing field lines then start inside the closed field structure and incorrectly flag it as open. However, since the magnetic island width is, at most, of the order of a few d_i, and since our analysis-box is $20d_i$ from the simulation boundary, our results are unaffected by such "boundary islands."

3. Results

3.1. Temporal Evolution of Shock-RD Interaction

The evolution of the system changes significantly depending on the shock and RD properties. This is exemplified in Figure 2, where the left and right columns contain snapshots from Runs 1 and 4, respectively. When the RD reaches the $Q_\perp$ shock (Figure 2b), the interaction mainly results in a smooth transition from a $Q_\perp$ to a $Q_\parallel$ shock geometry, without the excitation of additional large amplitude fluctuations. One notable feature of the interaction is that the tilt of the RD results in a temporary tilting of the shock surface (highlighted with the yellow dashed line). This is due to the $Q_\perp$ shock propagating faster than the newly forming $Q_\parallel$ shock (see Table 1). The portion of the shock that remains $Q_\perp$ for a longer time continues to move at its initial speed while the newly formed $Q_\parallel$ shock slows down. This causes the shock surface to tilt slightly toward the RD, thereby temporarily decreasing θ_{Bn}. After the transition to $Q_\parallel$ is complete, the tilt eventually disappears over $\sim 10\ \omega_{ci}^{-1}$.

The $Q_\parallel \rightarrow Q_\perp$ case (d–f) is very different. In the case of Run 4, a foreshock transient is formed around the RD once it reaches the foreshock, and the new $Q_\perp$ shock surface starts to form upstream of the transient (Figures 2e and 2f). A similar, but much smaller transient is formed in Run 3. Inside the transient, T increases significantly (Figure 3a) while the magnetic field magnitude $|\mathbf{B}|$, number density n, and v_x decrease (Figures 3c–3e, respectively). These properties are typical for both foreshock bubbles (FBs) (Omidi et al., 2010) and hot flow anomalies (HFAs) (Omidi & Sibeck, 2007). However, since the upstream discontinuity is an RD and the transient started growing once the RD reached the foreshock, it is likely that the transient is an FB (Omidi et al., 2010) and not an HFA, which are instead typically formed when a tangential discontinuity intersects a shock surface (Omidi & Sibeck, 2007). By extracting data along the virtual spacecraft trajectory shown in Figure 3a we can make a qualitative comparison between our simulations (Figures 3b–3e) and an FB observation made by the MMS spacecraft (Figures 3f–3i) reported by Turner et al. (2020).

While the two are qualitatively similar, there are some noticeable differences such as the shape of the FB core and the fact that the virtual spacecraft is in the foreshock prior to the FB whereas MMS was in the solar wind on both sides of the FB. Although the difference in core shape might to some extent be attributed to the relative motion between the spacecraft and the FB, the most likely source is the local nature of our model. Since we are not resolving the full shock we are always going to observe the initial growth-phase of the FB, and we are therefore limited to much smaller structures than usually observed in space. Indeed, an early stage FB reported by Madanian et al. (2023, Figure 3) at the Martian bow shock compares favorably with the FB core in our

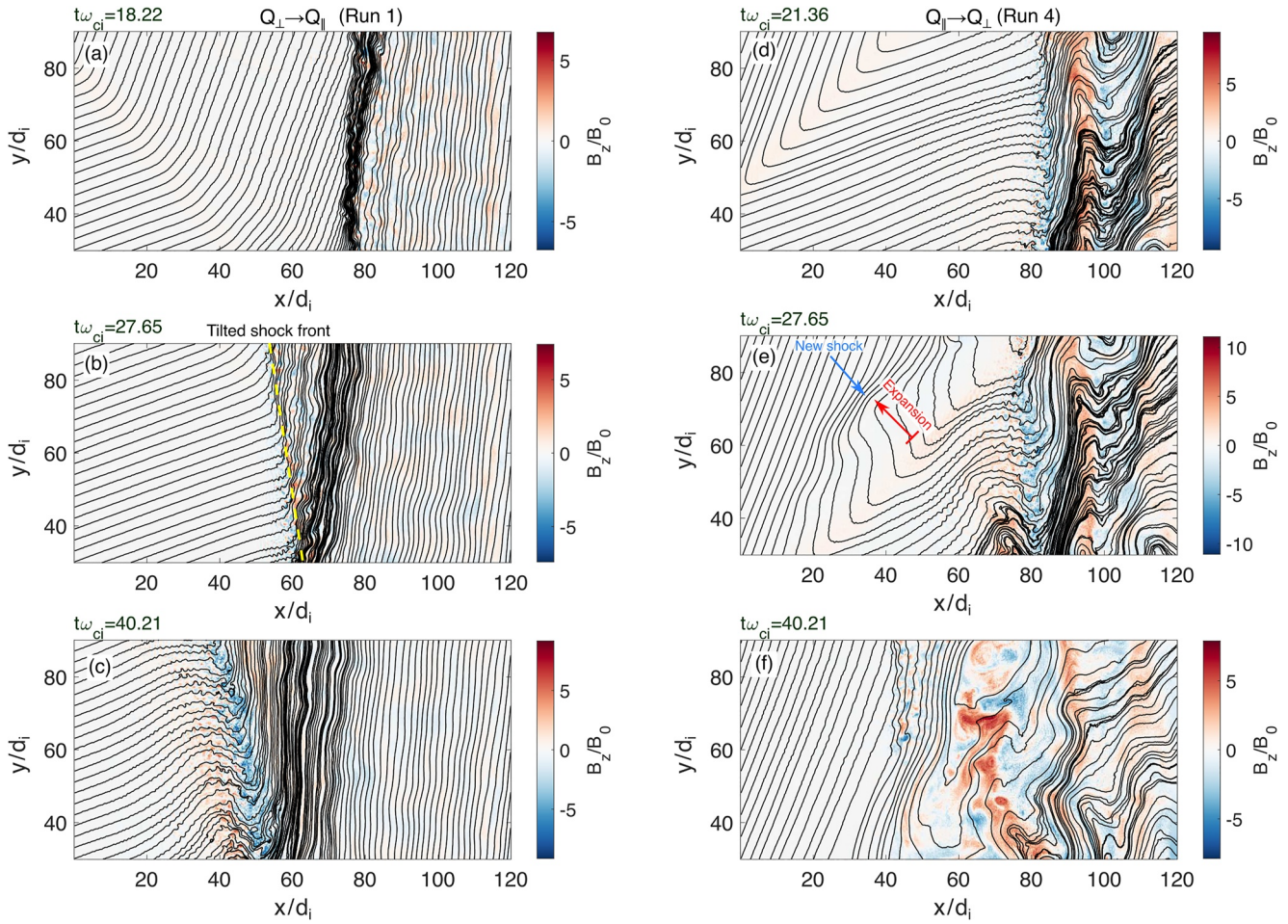

Figure 2. Two cases of shock-RD-interactions. (a–c) Temporal evolution of Run 1, color-coding B_z normalized to the upstream magnetic field strength B_0. (d–f) Same format as (a–c) for Run 4. Note that the starting points of the magnetic field lines are separated with distances irrespective of |**B**|. Hence, the "field line density" is not a consistent indicator of |**B**| across the whole domain, only locally.

simulations. Moreover, since we are not resolving the global curvature of bow shocks, any simple trajectory crossing the FB must either start or end in the foreshock. We conclude that, while there are some differences between our transients and typical FBs observed by spacecraft, the foreshock transients observed in our simulations are likely FBs in an early stage of their evolution. Eventually, the new $Q_\perp$ shock is fully formed, and remnants of the shock-RD interaction are only found downstream.

3.2. Occurrence of Closed Magnetic Field Structures

For each time step in each run, we perform the analysis discussed in Section 2.3 to determine the total area occupied by closed magnetic field structures. The results are summarized in Figure 4, which shows snapshots from Run 4 (Figures 4a–4c) as well as the total area occupied by closed field, A_{closed}, as a function of time for all runs (Figures 4d and 4e). Before the RD has interacted with the shock, our results reproduce the findings of Gingell et al. (2023), namely that the occurrence of reconnected structures heavily favors the $Q_\parallel$ geometry and larger M_A. Moreover, the good agreement between the two $Q_\parallel$ reference runs using periodic (light blue) and non-periodic (dark blue) y-boundaries indicates that edge effects only have minor influence on the results. Once the RDs reach the shocks, the response varies greatly depending on shock and RD properties.

To start, we focus on the runs where the shock is initially $Q_\parallel$ (Figure 4d). For all such runs, we find that closed field structures are produced once the foreshock has become well developed (i.e., after several ω_{ci}^{-1}). This process is faster for the high-M_A shock (Run 5, orange). The decrease in A_{closed} after the first peak in all runs is due to the

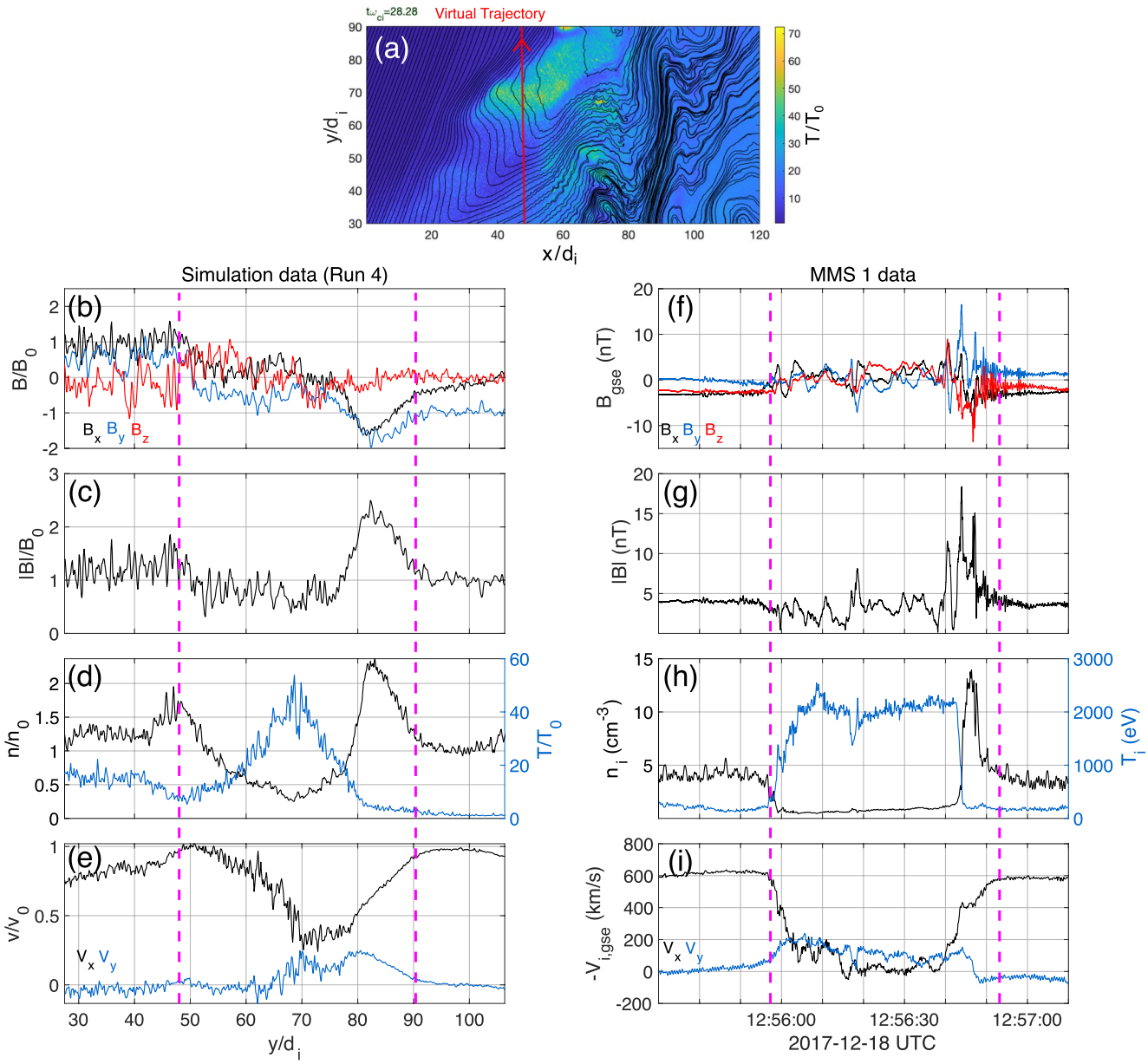

Figure 3. Observations of a foreshock transient in our local hybrid simulation and with Magnetospheric Multiscale. (a) Simulation slice from $t\omega_{ci} = 28.28$, with ion temperature color coded. (b–e) Portion of the simulation data gathered along the trajectory shown in red in panel (a). (b) Magnetic field vector components, (c) magnetic field magnitude, (d) density (black) and ion temperature (blue), (e) velocity components. (f–i) MMS 1 data of a foreshock bubble identified and analyzed by Turner et al. (2020) in the same format as panels (b–e), with vector quantities presented in the geocentric solar ecliptic (GSE) coordinate system. The magenta lines indicate roughly the FB boundaries.

combined effect of (a) cyclic shock reformation (Burgess, 1989) which temporarily stops the formation of new closed field structures, and (b) the decay of existing closed field structures as they propagate downstream (Gingell et al., 2023). Once the new foreshock is fully developed, the formation process resumes. Up to the point that the RD reaches the foreshock ($t\omega_{ci} \approx 20$ for the high M_A run, and ≈25 for the others), the $U_{in} = 6v_A$ runs (Runs 3, 4, 6, 7) are in very good agreement. This indicates that the random numerical noise in the simulations is small enough that the closed field analysis is stable to it. The runs deviate significantly from each other once the RDs arrive. In the $\Delta\varphi_B = 50°$ run (black), a negligible amount of A_{closed} is generated by the interaction of the RD with the shock, and the change to the $Q_\perp$ geometry stops the production of new closed field structures almost entirely. This resulting in a slow decrease of A_{closed} after the crossing. In stark contrast, we observe a burst of reconnection in the

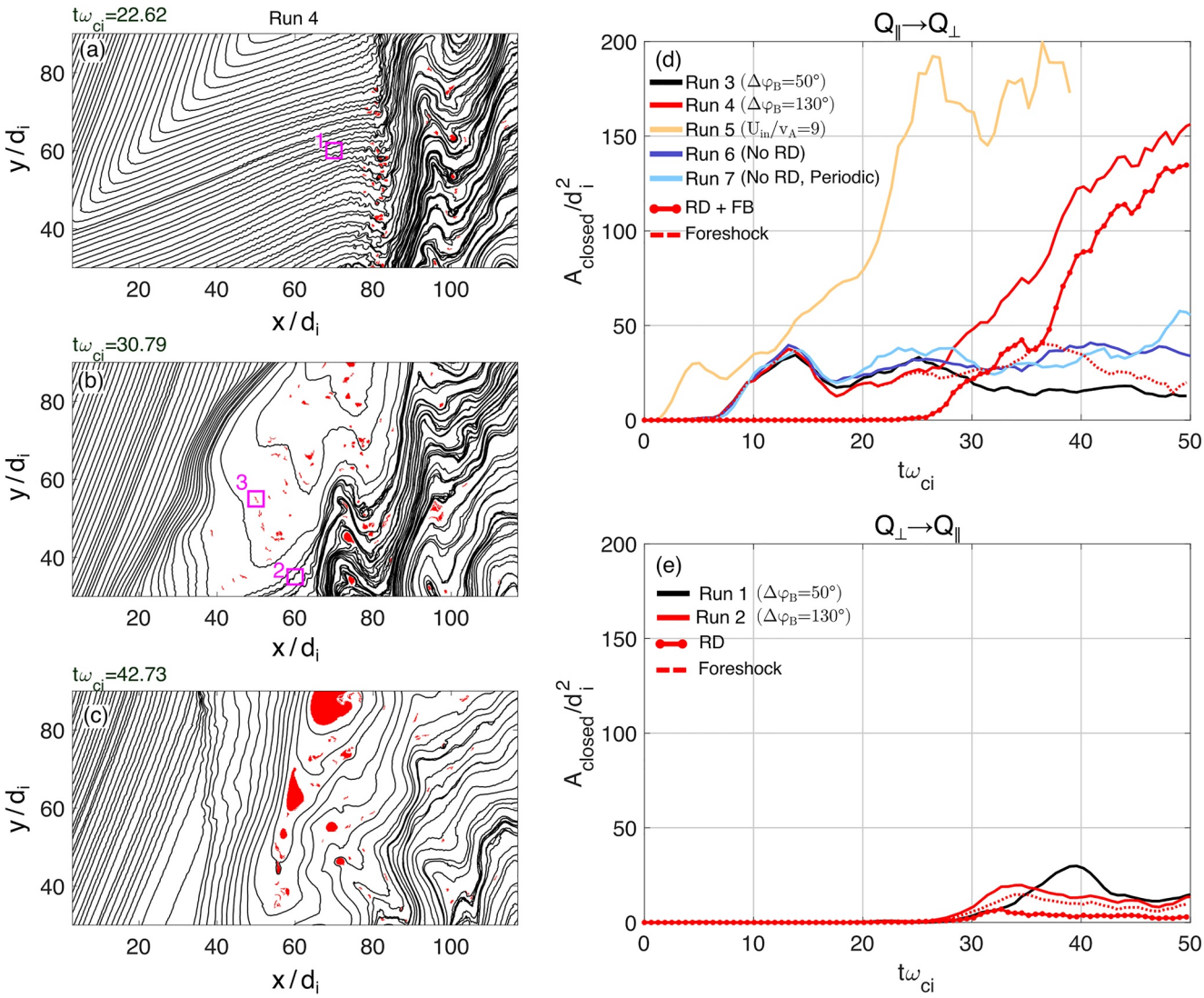

Figure 4. Closed field analysis. (a–c) Snapshots from the Run 4 (red line in panel d). Cells flagged as containing closed field are red. Magenta boxes in panels (a) and (b) show the regions over which the ion distributions are collected for Figure 5. (d) Total area occupied by closed field as a function of time for the $Q_{\parallel} \rightarrow Q_{\perp}$ runs 3 to 7. The circle-marked and dotted lines show the different contributions to the closed field for the run with corresponding color. A moving average over four points has been applied to reduce noise. (e) Same as (d) but for the $Q_{\perp} \rightarrow Q_{\parallel}$ runs 1 and 2.

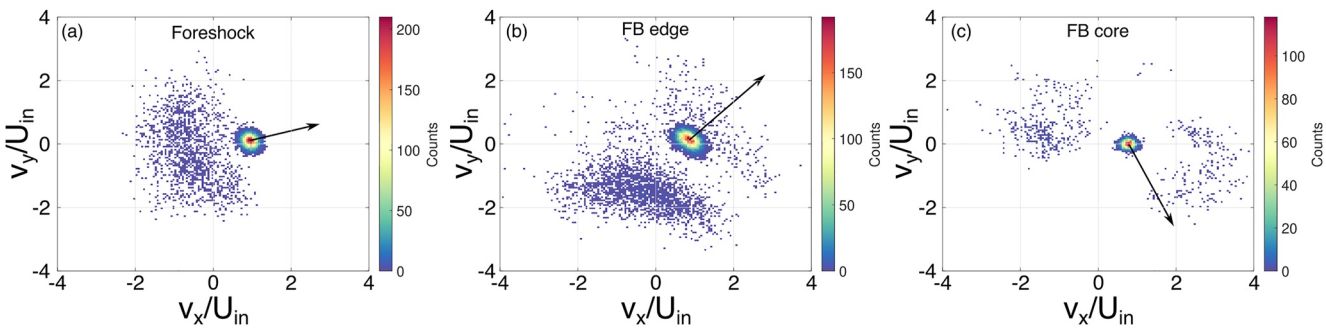

Figure 5. 2D ion velocity distributions. The data in panels a, b and c, are taken from the magenta boxes in Figures 4a and 4b, marked 1, 2, and 3, respectively. The velocities are given in the downstream frame, and the black arrow in each panel shows the local magnetic field direction.

$\Delta\varphi = 130°$ run (red) when the RD interacts with the foreshock. This burst is due to (a) reconnection inside the FB formed by the foreshock-RD interaction, and (b) internal reconnection of the RD current sheet. The FB-related closed field structures visible in Figure 4b are small in scale ($\sim 1 d_i$), comparable to the structures formed by the ordinary foreshock. This suggests that the generation mechanism is likely similar. The magnetic islands generated by internal reconnection of the RD seen in Figure 4c can be much larger, up to $\sim 10 d_i$.

As is clearly seen in Figures 4a–4c, closed field structures are formed when the shock is $Q_{\parallel}$ (Figure 4a) and when the RD interacts with the shock (Figures 4b and 4c). Once the shock becomes $Q_{\perp}$, no new closed field structures are formed due the absence of a foreshock (Figure 4c). Therefore, all closed field structures downstream of the RD are due to the original foreshock, and everything upstream or inside the RD is due to either the FB or RD. Thus, by manually splitting the domain slightly downstream of the RD (as identified in B_y) each time step, we can label any given closed field structure as being due to either the original foreshock or the shock-RD interaction (i.e., FB or RD), and we can qualitatively compare the different contributions. These contributions are plotted in Figure 4d as dotted (ordinary foreshock) and circle-marked (combined RD and FB) lines. We emphasize that the location of the RD was identified by eye, which means that there may be a small number of structures that are misidentified, and these lines should therefore be understood to be approximate. As the RD propagates into the downstream, it continues reconnecting, and A_{closed} remains large, even though the newly formed $Q_{\perp}$ shock geometry prevents the generation of new foreshock reconnection. The picture is essentially the same for the high-M_A (orange) case, except that the larger M_A run develops more closed area, consistent with the findings of Gingell et al. (2023). Our results clearly demonstrate that the RD properties have an important effect on the production of closed field structures, that is, on the occurrence of magnetic reconnection. Indeed, although we only capture the initial growth-phase of the FB, we still find a significant increase of reconnection compared to the steady upstream reference run.

The fact that the reconnection occurrence is different inside the FB compared to the ordinary foreshock is not surprising given the difference in plasma conditions (e.g., Figure 3). To understand why the FB results in an increased reconnection occurrence we examine, in Figure 5, the ion velocity distribution taken from different locations (see the magenta boxes in Figures 4a and 4b). The distribution in the ordinary foreshock (Figure 5a) contains the inflowing plasma and the reflected, backstreaming population. It is the interaction between these populations that eventually leads to the formation of thin current sheets and magnetic reconnection in the foreshock (Bessho et al., 2020; Gingell et al., 2017). As the FB develops and we approach its core from the downstream (Figure 5b), we start observing the presence of accelerated ions moving toward the shock. This population is likely the result of energetic ion leakage from the FB core (Liu et al., 2017). In the core (Figure 5c), we observe a population of high-energy ions streaming toward the shock. This population is a common feature of FB cores, and is the result of backstreaming ions being reflected by the new shock at the upstream edge of the FB (e.g., Liu et al., 2018; Omidi et al., 2010). Such an additional plasma component is a potential source of free energy for various plasma instabilities, which eventually could lead to the formation of small-scale current sheets and small-scale reconnection. This could thus naturally explain the observed enhancement of reconnection occurrence. We leave more detailed analysis of the instabilities and processes leading to the generation of the reconnecting current sheets inside the FBs for a future study.

Next, we focus on the initially $Q_{\perp}$ runs in Figure 4e. Before the RD reaches the shock, changing the shock geometry to $Q_{\parallel}$, we observe little to no reconnection as quantified by A_{closed}. This is expected for the plasma conditions under investigation, as discussed in the introduction and shown by Gingell et al. (2023). Due to the lack of foreshocks, neither run produces any foreshock transients when the RD interacts with the shock. In the $\Delta\varphi_B = 130°$ case (Run 2; red), we find that the RD compression leads to a small amount of internal RD reconnection, as indicated by the circle-marked line. At the same time, the change to a $Q_{\parallel}$ geometry starts the formation of a foreshock and subsequently of small scale reconnection sites, quantified by the dotted line. Interestingly, we see that while A_{closed} initially increases faster in the $\Delta\varphi_B = 130°$ run (red) than in the $\Delta\varphi_B = 50°$ run (black), it is overtaken at around $t\omega_{\text{ci}} = 35$ despite the $\Delta\varphi_B = 50°$ run showing no signs of reconnection within the RD. The reason for this is the shock tilting due to the RD orientation observed previously in Figure 2b. In the $\Delta\varphi_B = 50°$ case, this tilt is toward the new upstream magnetic field, causing a temporary and local decrease of θ_{Bn} and consequently enhanced reconnection. On the contrary, in the $\Delta\varphi_B = 130°$ case, the shock normal is tilted away from the upstream magnetic field, increasing θ_{Bn}, thereby reducing the occurrence of reconnection in the foreshock. Once this RD-induced tilt has been straightened out and the shock normal has returned to its initial direction, the two runs converge on each other again.

In summary, we find that the shock and RD properties have a large impact on the formation of reconnected magnetic structures. Particularly interesting is the case of a high magnetic shear RD interacting with a $Q_{\parallel}$ shock, as this setup gives rise to both small scale reconnection inside FBs and large scale reconnection of the RD itself. These results indicate that magnetic reconnection is likely to be a particularly important dissipation mechanism in such instances.

4. Summary and Conclusions

In the present paper we have modified a local 2.5D hybrid-PIC model (Gingell et al., 2023; Matthews, 1994) to study the interaction between collisionless shocks and upstream discontinuities. The focused scope of our local model enables us to study ion-scale shock processes more cost efficiently than global models. We apply the model to investigate the effect upstream rotational discontinuities (RDs) have on the occurrence of magnetic reconnection at collisionless shocks. In particular, we focus on RDs causing a transition between the quasi-parallel ($Q_{\parallel}$) and quasi-perpendicular ($Q_{\perp}$) shock geometries (corresponding to the most dramatic restructuring of the shock), using plasma parameters relevant for the Earth's bow shock. We find that significant bursts of magnetic reconnection, as quantified by the area occupied by reconnected magnetic structures, can occur during the $Q_{\parallel} \rightarrow Q_{\perp}$ transition if the magnetic shear across the RD is large. The burst occurs due to reconnection within the RD itself, and due to reconnection at kinetic-scale structures which are formed inside foreshock transients. For the cases discussed in this paper, we find that these transients are consistent with foreshock bubbles. A much smaller increase of reconnection is observed in the $Q_{\perp} \rightarrow Q_{\parallel}$ transition, where the absence of a pre-existing foreshock prevents the formation of FBs. Instead we find that, due to the different shock speeds, these transitions can cause a temporary tilt of the shock surface, leading to local variations in θ_{Bn}. These temporary variations in θ_{Bn} subsequently lead to a change in the occurrence of magnetic reconnection. We conclude that the presence of upstream RDs can greatly increase the occurrence of magnetic reconnection at collisionless shocks, primarily on the $Q_{\parallel}$ side. These results suggest that magnetic reconnection might be a particularly important dissipation mechanism for collisionless shocks during periods of dynamic upstream conditions.

In addition to the aforementioned results, the present work has opened the door to more comprehensive parametric studies in the future. It may be fruitful to expand the parameter space investigated in this study from Earth-like conditions to larger M_A values, where upstream waves with larger amplitude as well as stronger turbulence inhabit the foreshock. It could also be of interest to study the effects of other upstream structures such as tangential discontinuities, since they can lead to the formation of hot flow anomalies. Lastly, by building further on our model it should be possible to eventually investigate the ion physics of shock-shock collisions.

Data Availability Statement

The simulation data and MATLAB codes used to produce Figures 2–5 are publicly available at (Steinvall & Gingell, 2023). MMS data are publicly available at https://lasp.colorado.edu/mms/sdc/public/.

Acknowledgments
K. Steinvall and I. Gingell are supported by the Royal Society University Research Fellowship URF\R1\191547 and associated Royal Society Enhanced Research Expenses award RF\ERE\210405. The EPOCH code used in this work was in part funded by the UK EPSRC grants EP/G054950/1, EP/G056803/1, EP/G055165/1, EP/M022463/1 and EP/P02212X/1.

References

Arber, T. D., Bennett, K., Brady, C. S., Lawrence-Douglas, A., Ramsay, M. G., Sircombe, N. J., et al. (2015). Contemporary particle-in-cell approach to laser-plasma modelling. *Plasma Physics and Controlled Fusion*, *57*(11), 113001. https://doi.org/10.1088/0741-3335/57/11/113001

Bai, S.-C., Shi, Q., Liu, T. Z., Zhang, H., Yue, C., Sun, W.-J., et al. (2020). Ion-scale flux rope observed inside a hot flow anomaly. *Geophysical Research Letters*, *47*(5), e2019GL085933. https://doi.org/10.1029/2019GL085933

Bessho, N., Chen, L.-J., Hesse, M., Ng, J., Wilson, L. B., & Stawarz, J. E. (2023). Electron acceleration and heating during magnetic reconnection in the earth's quasi-parallel bow shock. *The Astrophysical Journal*, *954*(1), 25. https://doi.org/10.3847/1538-4357/ace321

Bessho, N., Chen, L.-J., Wang, S., Hesse, M., Wilson, L. B., & Ng, J. (2020). Magnetic reconnection and kinetic waves generated in the Earth's quasi-parallel bow shock. *Physics of Plasmas*, *27*(9). https://doi.org/10.1063/5.0012443

Birn, J., & Priest, E. R. (2007). *Reconnection of magnetic fields: Magnetohydrodynamics and collisionless theory and observations*. Cambridge University Press.

Burgess, D. (1989). Cyclic behavior at quasi-parallel collisionless shocks. *Geophysical Research Letters*, *16*(5), 345–348. https://doi.org/10.1029/GL016i005p00345

Burgess, D., & Scholer, M. (2015). *Collisionless shocks in space plasmas: Structure and accelerated particles*. Cambridge University Press.

Burlaga, L. F., Lemaire, J. F., & Turner, J. M. (1977). Interplanetary current sheets at 1 au. *Journal of Geophysical Research (1896-1977)*, *82*(22), 3191–3200. https://doi.org/10.1029/JA082i022p03191

Califano, F., Cerri, S. S., Faganello, M., Laveder, D., Sisti, M., & Kunz, M. W. (2020). Electron-only reconnection in plasma turbulence. *Frontiers in Physics*, *8*. https://doi.org/10.3389/fphy.2020.00317

Gingell, I., Schwartz, S. J., Burgess, D., Johlander, A., Russell, C. T., Burch, J. L., et al. (2017). MMS observations and hybrid simulations of surface ripples at a marginally quasi-parallel shock. *Journal of Geophysical Research: Space Physics*, *122*(11), 11003–11017. https://doi.org/10.1002/2017JA024538

Gingell, I., Schwartz, S. J., Eastwood, J. P., Burch, J. L., Ergun, R. E., Fuselier, S., et al. (2019). Observations of magnetic reconnection in the transition region of quasi-parallel shocks. *Geophysical Research Letters*, *46*(3), 1177–1184. https://doi.org/10.1029/2018GL081804

Gingell, I., Schwartz, S. J., Eastwood, J. P., Stawarz, J. E., Burch, J. L., Ergun, R. E., et al. (2020). Statistics of reconnecting current sheets in the transition region of earth's bow shock. *Journal of Geophysical Research: Space Physics*, *125*(1), e2019JA027119. https://doi.org/10.1029/2019JA027119

Gingell, I., Schwartz, S. J., Kucharek, H., Farrugia, C. J., Fryer, L. J., Plank, J., & Trattner, K. J. (2023). Hybrid simulations of the decay of reconnected structures downstream of the bow shock. *Physics of Plasmas*, *30*(1). https://doi.org/10.1063/5.0129084

Guo, A., Lu, Q., Lu, S., Wang, S., & Wang, R. (2023). Properties of electron-scale magnetic reconnection at a quasi-perpendicular shock. *The Astrophysical Journal*, *955*(1), 14. https://doi.org/10.3847/1538-4357/acec48

Guo, Z., Lin, Y., & Wang, X. (2021). Global hybrid simulations of interaction between interplanetary rotational discontinuity and bow shock/magnetosphere: Can ion-scale magnetic reconnection be driven by rotational discontinuity downstream of quasi-parallel shock? *Journal of Geophysical Research: Space Physics*, *126*(4), e2020JA028853. https://doi.org/10.1029/2020JA028853

Hamrin, M., Gunell, H., Goncharov, O., De Spiegeleer, A., Fuselier, S., Mukherjee, J., et al. (2019). Can reconnection be triggered as a solar wind directional discontinuity crosses the bow shock? A case of asymmetric reconnection. *Journal of Geophysical Research: Space Physics*, *124*(11), 8507–8523. https://doi.org/10.1029/2019JA027006

Hesse, M., & Cassak, P. A. (2020). Magnetic reconnection in the space sciences: Past, present, and future. *Journal of Geophysical Research: Space Physics*, *125*(2), e2018JA025935. https://doi.org/10.1029/2018JA025935

Karimabadi, H., Roytershteyn, V., Vu, H. X., Omelchenko, Y. A., Scudder, J., Daughton, W., et al. (2014). The link between shocks, turbulence, and magnetic reconnection in collisionless plasmas. *Physics of Plasmas*, *21*(6), 062308. https://doi.org/10.1063/1.4882875

Kennel, C., Edmiston, J., & Hada, T. (1985). *A quarter century of collisionless shock research* (Vol. 34, pp. 1–36). Washington DC American Geophysical Union Geophysical Monograph Series.

Knetter, T., Neubauer, F. M., Horbury, T., & Balogh, A. (2004). Four-point discontinuity observations using cluster magnetic field data: A statistical survey. *Journal of Geophysical Research*, *109*(A6). https://doi.org/10.1029/2003JA010099

Lin, Y. (1997). Generation of anomalous flows near the bow shock by its interaction with interplanetary discontinuities. *Journal of Geophysical Research*, *102*(A11), 24265–24281. https://doi.org/10.1029/97JA01989

Liu, T. Z., Angelopoulos, V., & Hietala, H. (2017). Energetic ion leakage from foreshock transient cores. *Journal of Geophysical Research: Space Physics*, *122*(7), 7209–7225. https://doi.org/10.1002/2017JA024257

Liu, T. Z., Lu, S., Angelopoulos, V., Lin, Y., & Wang, X. Y. (2018). Ion acceleration inside foreshock transients. *Journal of Geophysical Research: Space Physics*, *123*(1), 163–178. https://doi.org/10.1002/2017JA024838

Liu, T. Z., Lu, S., Turner, D. L., Gingell, I., Angelopoulos, V., Zhang, H., et al. (2020). Magnetospheric multiscale (MMS) observations of magnetic reconnection in foreshock transients. *Journal of Geophysical Research: Space Physics*, *125*(4), e2020JA027822. https://doi.org/10.1029/2020JA027822

Lu, Q., Yang, Z., Wang, H., Wang, R., Huang, K., Lu, S., & Wang, S. (2021). Two-dimensional particle-in-cell simulation of magnetic reconnection in the downstream of a quasi-perpendicular shock. *The Astrophysical Journal*, *919*(1), 28. https://doi.org/10.3847/1538-4357/ac18c0

Madanian, H., Omidi, N., Sibeck, D. G., Andersson, L., Ramstad, R., Xu, S., et al. (2023). Transient foreshock structures upstream of mars: Implications of the small martian bow shock. *Geophysical Research Letters*, *50*(8), e2022GL101734. https://doi.org/10.1029/2022GL101734

Matsumoto, Y., Amano, T., Kato, T. N., & Hoshino, M. (2015). Stochastic electron acceleration during spontaneous turbulent reconnection in a strong shock wave. *Science*, *347*(6225), 974–978. https://doi.org/10.1126/science.1260168

Matthews, A. P. (1994). Current advance method and cyclic leapfrog for 2d multispecies hybrid plasma simulations. *Journal of Computational Physics*, *112*(1), 102–116. https://doi.org/10.1006/jcph.1994.1084

Omidi, N., Eastwood, J. P., & Sibeck, D. G. (2010). Foreshock bubbles and their global magnetospheric impacts. *Journal of Geophysical Research*, *115*(A6). https://doi.org/10.1029/2009JA014828

Omidi, N., Lee, S. H., Sibeck, D. G., Turner, D. L., Liu, T. Z., & Angelopoulos, V. (2020). Formation and topology of foreshock bubbles. *Journal of Geophysical Research: Space Physics*, *125*(9), e2020JA028058. https://doi.org/10.1029/2020JA028058

Omidi, N., & Sibeck, D. G. (2007). Formation of hot flow anomalies and solitary shocks. *Journal of Geophysical Research*, *112*(A1). https://doi.org/10.1029/2006JA011663

Phan, T. D., Eastwood, J. P., Shay, M. A., Drake, J. F., Sonnerup, B. U. Ö., Fujimoto, M., et al. (2018). Electron magnetic reconnection without ion coupling in Earth's turbulent magnetosheath. *Nature*, *557*(7704), 202–206. https://doi.org/10.1038/s41586-018-0091-5

Richter, P., & Scholer, M. (1989). On the stability of rotational discontinuities. *Geophysical Research Letters*, *16*(11), 1257–1260. https://doi.org/10.1029/GL016i011p01257

Schwartz, S. J., Kucharek, H., Farrugia, C. J., Trattner, K., Gingell, I., Ergun, R. E., et al. (2021). Energy conversion within current sheets in the earth's quasi-parallel magnetosheath. *Geophysical Research Letters*, *48*(4), e2020GL091859. https://doi.org/10.1029/2020GL091859

Steinvall, K., & Gingell, I. (2023). Simulation data archive: The influence of rotational discontinuities on the formation of reconnected structures at collisionless shocks – Hybrid simulations (version v2) [Dataset]. Zenodo. https://doi.org/10.5281/zenodo.10171257

Turner, D. L., Liu, T. Z., Wilson, L. B., III, Cohen, I. J., Gershman, D. G., Fennell, J. F., et al. (2020). Microscopic, multipoint characterization of foreshock bubbles with magnetospheric multiscale (MMS). *Journal of Geophysical Research: Space Physics*, *125*(7), e2019JA027707. https://doi.org/10.1029/2019JA027707

Vasko, I. Y., Alimov, K., Phan, T., Bale, S. D., Mozer, F. S., & Artemyev, A. V. (2022). Kinetic-scale current sheets in the solar wind at 1 au: Scale-dependent properties and critical current density. *The Astrophysical Journal Letters*, *926*(2), L19. https://doi.org/10.3847/2041-8213/ac4fc4

Wang, S., Chen, L.-J., Bessho, N., Hesse, M., Wilson, L. B., III, Giles, B., et al. (2019). Observational evidence of magnetic reconnection in the terrestrial bow shock transition region. *Geophysical Research Letters*, *46*(2), 562–570. https://doi.org/10.1029/2018GL080944

Zhang, H., Zong, Q., Connor, H., Delamere, P., Facskó, G., Han, D., et al. (2022). Dayside transient phenomena and their impact on the magnetosphere and ionosphere. *Space Science Reviews*, *218*(5), 40. https://doi.org/10.1007/s11214-021-00865-0